

Recognition of Lung Cancers on CT Using 3-D Object Models of Different Classes

Hotaka Takizawa
University of Tsukuba
305-8573, JAPAN
takizawa@cs.tsukuba.ac.jp

Shinji Yamamoto
Chukyo University
470-0393, JAPAN

Tsuyoshi Shiina
Kyoto University
606-8507, JAPAN

Abstract

The present paper describes a recognition method of pulmonary nodules in thoracic CT scans by use of 3-D spherical and cylindrical models that represent nodules (i.e. possible cancers) and blood vessels, respectively. The anatomical validity of these object models and their fidelity to CT scans are evaluated based on the Bayes theorem. The nodule recognition is employed by the maximum a posteriori estimation. The proposed method is applied to actual CT scans, and experimental results are shown.

1 Introduction

Lung cancer is the most common cause of death among all cancers worldwide. To cope with this serious problem, mass screening for lung cancer has been widely performed by simple X-ray films with sputum cytological tests. However, it is known that the accuracy of this method is not sufficient for early detection of lung cancer. Therefore, a lung cancer screening system by CT for mass screening is proposed. This system improves the accuracy of the cancer detection considerably, but has one problem that the number of the images is increased to over dozens of slice sections per patient from 1 X-ray film. It is difficult for a radiologist (i.e. a medical doctor who specializes in reading radiographs) to interpret all the images in a limited time. In order to make the system more practical, it is necessary to develop a computer-aided diagnosis (CAD) system that automatically detects pathologic candidate regions suspected to comprise pulmonary nodules, and informs a radiologist of their positions in CT scans as a *second opinion*.

In the present paper, we propose a novel recognition method of pulmonary nodules in thoracic CT scans by use of 3-D deformable spherical and cylindrical models that represent nodules and blood vessels, respectively. The anatomical validity of the object models are evaluated by the probability distributions of the parameters of the object models. The probability distribution are predefined considering the anatomy. The fidelity of the object models to CT scans are also evaluated by use of the differences in intensity distribution between the CT scans and template images that are produced from the object models by a computer graphics technique. Through these evaluations, the posteriori probabilities of hypotheses that the object models appear in a CT scan are calculated on the basis of the Bayes theorem. From the most likely object model obtained by the MAP estimation, it is determined whether or not the CT scan is pathological.

2 3-D Deformable Object Models

2.1 Nodule

A nodule is represented by a spherical model as shown in Fig.1(a). The center position, radius and X-ray attenuation of a nodule model are denoted by $\mathbf{x}^N = (x^N, y^N, z^N)$, r^N and α_m^N , respectively. The X-ray attenuation of an area surrounding the nodule model (such an area is often called an *air* area) is denoted by α_a^N .

In medical diagnosis, the size of a nodule is the most important indicator to determine the stage of disease. Therefore, the radius r^N is more essential to describe a nodule than the other parameters \mathbf{x}^N , α_m^N and α_a^N . In the present paper, the former (i.e. r^N) and latter are called *essential* and *auxiliary* parameters, respectively. A nodule model is denoted by $o^N(r^N; \mathbf{x}^N, \alpha_m^N, \alpha_a^N)$, where the essential parameter is placed on the left-hand side of the semicolon. The probability density value of a hypothesis that a nodule model appears in a volume of interest (VOI) is defined by

$$p(o^N(r^N; \mathbf{x}^N, \alpha_m^N, \alpha_a^N)) = P^N \cdot g(r^N; \mu_r^N, \sigma_r^N), \quad (1)$$

where P^N is the appearance probability of the set of all possible nodules, and $g(x; \mu_x, \sigma_x)$ is a Gaussian distribution with a mean μ_x and standard deviation σ_x .

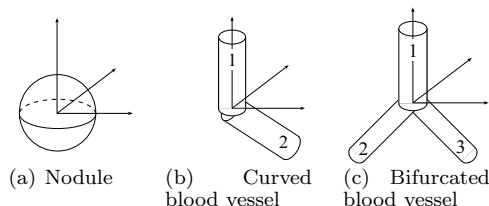


Figure 1: 3-D Object models.

2.2 Curved blood vessel

A curved section in a blood vessel tree is represented by two-connected-cylinder models as shown in Fig.1(b). The first cylinder corresponds to a parent vessel (indicated by '1'), which is nearer to a heart in respect of its blood flow, and the second its child vessel ('2'). The i -th cylinder ($i = 1, 2$) is represented by the radius r_i^{Bc} , zenith and azimuth angles, θ_i^{Bc} and

$\phi_i^{B_c}$. The connecting point of the two cylinders is represented by $\mathbf{x}^{B_c} = (x^{B_c}, y^{B_c}, z^{B_c})$. The X-ray attenuation of the model and its surrounding area are represented by $\alpha_m^{B_c}$ and $\alpha_a^{B_c}$, respectively. From these parameters, two additional parameters are calculated: the difference in section area between the cylinders δ^{B_c} and the angle between the two cylinders ψ^{B_c} . Because the parameters $r_1^{B_c}$, δ^{B_c} and ψ^{B_c} are thought to be more essential, a curved blood vessel model is denoted by $o^{B_c}(r_1^{B_c}, \delta^{B_c}, \psi^{B_c}; \mathbf{x}^{B_c}, r_2^{B_c}, \theta_1^{B_c}, \phi_1^{B_c}, \theta_2^{B_c}, \phi_2^{B_c}, \alpha_m^{B_c}, \alpha_a^{B_c})$.

The probability density value of appearance of a curved blood vessel model $o^{B_c}(r_1^{B_c}, \delta^{B_c}, \psi^{B_c}; \dots)$ is defined by

$$\begin{aligned} & p(o^{B_c}(r_1^{B_c}, \delta^{B_c}, \psi^{B_c}; \dots)) \\ &= P^{B_c} \cdot g(r_1^{B_c}; \mu_{r_1}^{B_c}(\mathbf{x}^{B_c}), \sigma_{r_1}^{B_c}) \cdot \\ & g(\delta^{B_c}; \mu_{\delta}^{B_c}, \sigma_{\delta}^{B_c}) \cdot g(\psi^{B_c}; \mu_{\psi}^{B_c}, \sigma_{\psi}^{B_c}), \quad (2) \end{aligned}$$

where P^{B_c} is the appearance probability of the set of all possible curved sections in blood vessel trees. The mean radius of a blood vessel $\mu_{r_1}^{B_c}(\mathbf{x}^{B_c})$ is defined as being the function of its position \mathbf{x}^{B_c} so as to represent the relationship between the radius and position in a lung region.

2.3 Bifurcated blood vessel

A bifurcation in a blood vessel tree is represented by three-connected-cylinder models as shown in Fig.1(c).

The probability density of appearance of a bifurcated blood vessel model $o^{B_b}(r_1^{B_b}, \delta_{23}^{B_b}, \delta_{123}^{B_b}, \psi_{12}^{B_b}, \psi_{13}^{B_b}, \psi_{23}^{B_b}; \dots)$ is defined in the same manner as a curved blood vessel as follows:

$$\begin{aligned} & p(o^{B_b}(r_1^{B_b}, \delta_{23}^{B_b}, \delta_{123}^{B_b}, \psi_{12}^{B_b}, \psi_{13}^{B_b}, \psi_{23}^{B_b}; \dots)) \\ &= P^{B_b} \cdot g(r_1^{B_b}; \mu_{r_1}^{B_b}(\mathbf{x}^{B_b}), \sigma_{r_1}^{B_b}) \cdot \\ & g(\delta_{23}^{B_b}; \mu_{\delta_{23}}^{B_b}, \sigma_{\delta_{23}}^{B_b}) \cdot g(\delta_{123}^{B_b}; \mu_{\delta_{123}}^{B_b}, \sigma_{\delta_{123}}^{B_b}) \cdot \\ & g(\psi_{12}^{B_b}; \mu_{\psi_{12}}^{B_b}, \sigma_{\psi_{12}}^{B_b}) \cdot g(\psi_{13}^{B_b}; \mu_{\psi_{13}}^{B_b}, \sigma_{\psi_{13}}^{B_b}) \cdot \\ & g(\psi_{23}^{B_b}; \mu_{\psi_{23}}^{B_b}, \sigma_{\psi_{23}}^{B_b}), \quad (3) \end{aligned}$$

where P^{B_b} is the appearance probability of the set of all possible bifurcations in blood vessel trees, $\delta_{23}^{B_b}$ is the difference in section area between the two child cylinders, $\delta_{123}^{B_b}$ is the difference in section area between the parent and child cylinders, that is $\delta_{123}^{B_b} = \pi((r_1^{B_b})^2 - (r_2^{B_b})^2 - (r_3^{B_b})^2)$, and $\psi_{ij}^{B_b}$ is the angle between the i -th and j -th cylinder ($i, j = 1, 2, 3, i \neq j$).

The appearance probabilities P^N , P^{B_c} and P^{B_b} satisfy the following equation:

$$\sum_{\tau \in \{N, B_c, B_b\}} P^\tau = 1, \quad (4)$$

where τ represents the class of an object model.

3 Modification of probability distribution of 3-D object models possessing different parameter spaces

The object models have the different essential parameters in number and type. For example, the nodule model has only one essential parameter r^N , whereas

the bifurcated blood vessel model has six other essential parameters $r_1^{B_b}$, $\delta_{23}^{B_b}$, $\delta_{123}^{B_b}$, $\psi_{12}^{B_b}$, $\psi_{13}^{B_b}$ and $\psi_{23}^{B_b}$. The differences in number cause a problem that generally, the probabilities of the object models that have more essential parameters are relatively underestimated.

Let us consider an example case where all the standard deviations are 1 and all the set appearance probabilities are 1/3. The probability of the nodule model whose r^N is $\mu + 3$, and that of the bifurcated blood vessel model whose essential parameters are μ 's are calculated as follows:

$$p(o^N) = 1/3 \cdot g(\mu + 3; \mu, 1) \approx 0.00148, \quad (5)$$

$$p(o^{B_b}) = 1/3 \cdot (g(\mu; \mu, 1))^6 \approx 0.00134. \quad (6)$$

Although the bifurcated blood vessel model has much more likely parameters, its probability is smaller than that of the nodule model.

Here, let us give a more generalized expression to the model probabilities as follows:

$$p(o^\tau(\boldsymbol{\omega}^\tau)) = P^\tau \cdot p(\boldsymbol{\omega}^\tau), \quad (7)$$

where $o^\tau(\boldsymbol{\omega}^\tau)$ represents an object model that has an essential parameter vector:

$$\boldsymbol{\omega}^\tau = \left(\omega_1^\tau \in \Omega_1^\tau, \omega_2^\tau \in \Omega_2^\tau, \dots, \omega_d^\tau \in \Omega_d^\tau, \dots, \omega_{D^\tau}^\tau \in \Omega_{D^\tau}^\tau \right) \in \Omega^\tau. \quad (8)$$

Ω^τ is the parameter space, and D^τ is its dimension. For example, $r_1^{B_c}$, δ^{B_c} and ψ^{B_c} in Eq.(2) correspond to $\omega_1^{B_c}$, $\omega_2^{B_c}$ and $\omega_3^{B_c}$, respectively, and the dimension D^{B_c} is 3. In Eq.(7), the auxiliary parameters are omitted for simplicity. The differences in the dimension D^τ between the model classes τ cause underestimation in $p(\boldsymbol{\omega}^\tau)$.

One solution to correct the underestimation is to use the geometric average of the parameter probability: ${}^{D^\tau}\sqrt{p(\boldsymbol{\omega}^\tau)}$, that is adopted in, for example, recognition of language [1] and speech [2]. Because the dimension D^τ is normalized, the underestimation is no longer caused. However, the geometrically averaged probability causes another problem that generally, the integral of its distribution over the parameter space

is not one: $\int_{\boldsymbol{\omega} \in \Omega^\tau} {}^{D^\tau}\sqrt{p(\boldsymbol{\omega})} d\boldsymbol{\omega} \neq 1$. We desire a

probability distribution that does not cause underestimation and that integrates to one. In this paper, we realize the desired probability distribution on a parameter space that is inhomogeneously divided so that the desired distribution may approximate to its geometrically averaged distribution.

First, each Ω_d^τ is divided into K isometric intervals $\Delta\Omega_d^\tau(k)$ ($k = 1, 2, \dots, K$) as shown in Fig.2. The interval size $|\Delta\Omega_d^\tau(k)|$ is equivalent to $\frac{|\Omega_d^\tau|}{K}$. By combining

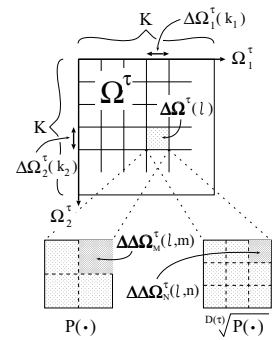


Figure 2: Division of a parameter space.

$\Delta\Omega_d^\tau(k)$, the following subspaces are generated:

$$\Delta\Omega^\tau(l) = \Delta\Omega_1^\tau(k_1) \times \Delta\Omega_2^\tau(k_2) \times \cdots \times \Delta\Omega_{D^\tau}^\tau(k_{D^\tau}), \quad (9)$$

where $l = 1, 2, \dots, K^{D^\tau}$. The operator $A \times B$ yields a product space of A and B . If K is enough large, then the probability distribution $p(\omega)$ can be regarded as being constant in $\Delta\Omega^\tau(l)$. Let $p^\tau(l)$ denote its constant value in $\Delta\Omega^\tau(l)$. The probability of $\Delta\Omega^\tau(l)$ is calculated as

$$P(\Delta\Omega^\tau(l)) = \int_{\Delta\Omega^\tau(l)} p(\omega) d\omega \approx p^\tau(l) \cdot |\Delta\Omega^\tau(l)|. \quad (10)$$

Then, two types of further division are made for each subspace $\Delta\Omega^\tau(l)$. One is the division into $M^\tau(l)$ isometric subsubspaces $\Delta\Delta\Omega_M^\tau(l, m)$ ($m = 1, 2, \dots, M^\tau(l)$), and the other is the division into N isometric subsubspaces $\Delta\Delta\Omega_N^\tau(l, n)$ ($n = 1, 2, \dots, N$) as shown in Fig.2. The subsubspace sizes $|\Delta\Delta\Omega_M^\tau(l, m)|$ and $|\Delta\Delta\Omega_N^\tau(l, n)|$ are equivalent to $\frac{|\Delta\Omega^\tau(l)|}{M^\tau(l)}$ and $\frac{|\Delta\Omega^\tau(l)|}{N}$, respectively. The division number N is constant, whereas $M^\tau(l)$ varies with τ and l . Therefore, the parameter space composed of $\Delta\Delta\Omega_M^\tau(l, m)$ is inhomogeneous. On the inhomogeneously divided parameter space, the desired probability distribution is defined as follows:

$$\begin{aligned} P(\Delta\Delta\Omega_M^\tau(l, m)) &= \frac{P(\Delta\Omega^\tau(l))}{M^\tau(l)} \\ &\approx \frac{p^\tau(l) \cdot |\Delta\Omega^\tau(l)|}{M^\tau(l)} = \frac{p^\tau(l) \cdot |\Omega^\tau|}{M^\tau(l) \cdot K^{D^\tau}}. \end{aligned} \quad (11)$$

On the other hand, on the parameter space composed of $\Delta\Delta\Omega_N^\tau(l, n)$, the geometrically averaged probability distribution is defined as follows:

$$\begin{aligned} Q(\Delta\Delta\Omega_N^\tau(l, n)) &= \frac{D^\tau \sqrt{P(\Delta\Omega^\tau(l))}}{N} \\ &\approx \frac{1}{N} \cdot D^\tau \sqrt{p^\tau(l) \cdot |\Delta\Omega^\tau(l)|} \\ &= \frac{1}{N} \cdot D^\tau \sqrt{p^\tau(l) \cdot \frac{|\Omega^\tau|}{K^{D^\tau}}} = \frac{D^\tau \sqrt{p^\tau(l) \cdot |\Omega^\tau|}}{N \cdot K}. \end{aligned} \quad (12)$$

Because the dimension D^τ is normalized in $D^\tau \sqrt{p^\tau(l)}$ and $D^\tau \sqrt{|\Omega^\tau|}$, the underestimation is not caused in $Q(\Delta\Delta\Omega_N^\tau(l, n))$.

By setting M as follows:

$$M^\tau(l) = \left\lfloor N \left(\frac{p^\tau(l) \cdot |\Omega^\tau|}{K^{D^\tau}} \right)^{1 - \frac{1}{D^\tau}} \right\rfloor \quad (13)$$

with an enough large number N , $P(\Delta\Delta\Omega_M^\tau(l, m))$ approximates to $Q(\Delta\Delta\Omega_N^\tau(l, n))$. In Eq.(13), $\lfloor x \rfloor$ is the nearest integer value of x . Consequently, we obtain the probability distribution that suppresses the underestimation and integrates to approximately one.

Let $O^\tau(\Delta\Delta\Omega_M^\tau(l, m))$ denote a set of the object models as follows:

$$O^\tau(\Delta\Delta\Omega_M^\tau(l, m)) = \{o^\tau(\omega^\tau) | \omega^\tau \in \Delta\Delta\Omega_M^\tau(l, m)\}. \quad (14)$$

The following probability distribution of the object model set:

$$P(O^\tau(\Delta\Delta\Omega_M^\tau(l, m))) = P^\tau \cdot P(\Delta\Delta\Omega_M^\tau(l, m)) \quad (15)$$

is used instead of $p(o^\tau(\omega^\tau))$ as a priori probability distribution in the Bayes formula.

4 Observation model

The Bayes formula also uses a likelihood function, that evaluates the fidelity of the object model to a CT VOI and is defined as the conditional probability of the CT VOI given the object model. To evaluate the fidelity, a template VOI is produced from the object model by simulating the CT imaging process where nodules and blood vessels are observed as regions with particular shapes on CT slice sections. The conditional probability is formulated by use of similarity between the CT VOI and the template VOI.

4.1 Production of templates from 3-D object models

Let $v_T(x, y, z; o^\tau(\omega^\tau))$ denote a voxel value at x, y, z in a template VOI. The value is calculated as

$$v_T(x, y, z; o^\tau(\omega^\tau)) = \alpha_m^\tau \cdot \zeta_m^\tau + \alpha_a^\tau \cdot (\zeta_v - \zeta_m^\tau), \quad (16)$$

where α_m^τ and α_a^τ are the X-ray attenuation of the object model and that of its surrounding area, respectively. ζ_v and ζ_m^τ are the volume of the whole voxel and that of a part where the object model intersects with the voxel, respectively.

4.2 Likelihood of VOIs to 3-D object models

The fidelity of the object model to a CT VOI is evaluated by the following correlation coefficient between the CT VOI and the template VOI:

$$\begin{aligned} \gamma(v_C, v_T) &= \frac{\sum_{x,y,z} (v_C(x, y, z) - \bar{v}_C) (v_T(x, y, z) - \bar{v}_T)}{\sqrt{\sum_{x,y,z} (v_C(x, y, z) - \bar{v}_C)^2} \sqrt{\sum_{x,y,z} (v_T(x, y, z) - \bar{v}_T)^2}}, \end{aligned} \quad (17)$$

where $v_C(x, y, z)$ is the voxel value at x, y, z in the CT VOI. \bar{v}_C and \bar{v}_T are the mean voxel values of the CT VOI and template VOI, respectively.

The correlation coefficient $\gamma(v_C, v_T)$ takes a value between 1 and -1. The higher the fidelity is, the larger the correlation coefficient is. The likelihood is defined as

$$p(v_C | o^\tau(\omega^\tau)) = \frac{\gamma(v_C, v_T) + 1}{2}. \quad (18)$$

5 Recognition of nodules based on the MAP estimation

Given a CT VOI v_C , the posteriori probability of the hypothesis that an object model set $O^\tau(\Delta\Delta\Omega_M^\tau(l, m))$

appears in the VOI is given by

$$\begin{aligned} & P(O^\tau(\Delta\Delta\Omega_M^\tau(l, m)|v_C)) \\ &= \int_{\Delta\Delta\Omega_M^\tau(l, m)} p(o^\tau(\omega)|v_C) d\omega \\ &= \int_{\Delta\Delta\Omega_M^\tau(l, m)} \beta \cdot p(v_C|o^\tau(\omega)) p(o^\tau(\omega)) d\omega, \quad (19) \end{aligned}$$

where $\beta = [p(v_C)]^{-1}$. In Eq.(19), the Bayes formula:

$$p(o^\tau(\omega)|v_C) = \beta \cdot p(v_C|o^\tau(\omega)) p(o^\tau(\omega)) \quad (20)$$

is used. Since the size of $\Delta\Delta\Omega_M^\tau(l, m)$ is small, the likelihood function $p(v_C|o^\tau(\omega))$ can be regarded as being constant in $\Delta\Delta\Omega_M^\tau(l, m)$. Thus,

$$\begin{aligned} & \text{the last term in Eq.(19)} \\ & \approx \beta \cdot p(v_C|o^\tau(\tilde{\omega}^\tau)) \int_{\Delta\Delta\Omega_M^\tau(l, m)} p(o^\tau(\omega)) d\omega \\ &= \beta \cdot p(v_C|o^\tau(\tilde{\omega}^\tau)) P(O^\tau(\Delta\Delta\Omega_M^\tau(l, m))), \quad (21) \end{aligned}$$

where $\tilde{\omega}^\tau$ is a certain essential parameter in $\Delta\Delta\Omega_M^\tau(l, m)$. The likelihood $p(v_C|o^\tau(\tilde{\omega}^\tau))$ and the priori probability $P(O^\tau(\Delta\Delta\Omega_M^\tau(l, m)))$ are obtained from Eqs.(18) and (15), respectively.

For each class $\tau = \{N, B_c, B_b\}$, the optimal essential parameter vector that maximizes the posteriori probability is obtained by the Powell method as follows:

$$(l^{\tau*}, m^{\tau*}) = \arg \max_{l, m} P(O^\tau(\Delta\Delta\Omega_M^\tau(l, m)|v_C)). \quad (22)$$

From the following ratio between the posteriori probabilities:

$$\rho(v_C) = \frac{P(O^N(\Delta\Delta\Omega_M^N(l^{N*}, m^{N*})|v_C))}{\max_{\tau \neq N} P(O^\tau(\Delta\Delta\Omega_M^\tau(l^{\tau*}, m^{\tau*})|v_C))}, \quad (23)$$

the CT VOI v_C is determined to be pathological if $\rho(v_C) \geq T_\rho$ and to be normal if $\rho(v_C) < T_\rho$ with a certain threshold T_ρ .

6 Experimental results

In this experiment, 26 thoracic CT scans are used with 30 actual pulmonary nodules. One slice cross section contains 512×512 pixels. From the CT scans, lung regions are extracted by a threshold-based technique [3], and then nodule candidates are detected by methods [4]. The number of nodule candidates is 93.8 per scan. They are composed of 28 actual nodules (two false negatives occurs) and 92.8 false positives per scan. By applying the method proposed in this paper to the nodule candidates with $T_\rho = 0.954$ that is determined

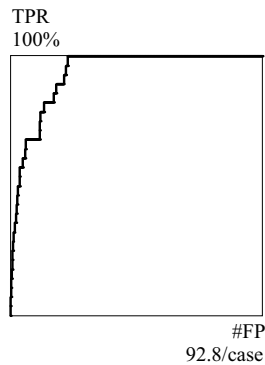


Figure 3: The fROC curve of the proposed method.

experimentally, the number of the false positives is successfully decreased to 21.2 per case without generating additional false negatives. The appearance probabilities P^N , P^{B_c} and P^{B_b} are set uniformly. Fig.3 show a fROC curve of the proposed method.

The false positive number obtained by our previous methods, such as [5], that use the ordinary joint probability is 61.2 at the true positive rate of 100%. The proposed method is more accurate than our previous methods.

Fig.4 shows a sample CT scan with a nodule that is identified by a radiologist and is also detected by the detection methods as a nodule candidate. Its diameter is about 4.5mm. The posteriori probabilities of the most likely object models o^N , o^{B_c} and o^{B_b} are 0.114, 0.100 and 0.100, respectively (the common constant values are omitted), and the ratio of the posteriori probabilities ρ is 1.14. Because the ratio is larger than the threshold T_ρ , the nodule candidate is correctly determined to be a nodule. The calculation time per candidate is approximately 40 second.

7 Conclusion

The present paper described a novel recognition method of pulmonary nodules in thoracic CT scans using 3-D deformable object models of different classes. The anatomical validity of these object models and their fidelity to CT scans were evaluated based on the Bayes inference. The nodule recognition was employed by the maximum a posteriori estimation. The experimental results were shown.

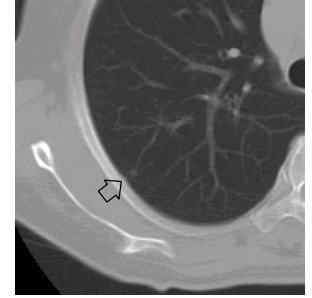


Figure 4: A sample thoracic CT scan. The arrow indicates a nodule that is identified by a radiologist.

References

- [1] Hang Li. "A probabilistic disambiguation method based on psycholinguistic". In *Proceedings of the 4th Workshop on Very Large Corpora*, pp. 141–154, 1996.
- [2] G.Li, et al. "An Improved Training Algorithm in HMM-based Speech Recognition". In *4th International Conference on Spoken Language Processing*, Vol. 2, pp. 1057–106, 2006.
- [3] S.Yamamoto, et al. "Image Processing for Computer-Aided Diagnosis of Lung Cancer by CT(LSCT)". *Systems and Computers in Japan*, Vol. 25, No. 2, pp. 67–80, 1994.
- [4] G.Fukano, H.Takizawa, S.Yamamoto, et al. "Eigen Image Recognition of Pulmonary Nodules from Thoracic CT Images by Use of Subspace Method". *IEICE Transactions on Information and Systems*, Vol. E88-D-II, No. 6, pp. 1273–1283, 2005.
- [5] H.Takizawa, S.Yamamoto, et al. "Recognition of Lung Cancers from X-ray CT Images Considering 3-D Structure of Objects and Uncertainty of Recognition". In *Proc. of Image Processing, part of SPIE*, Vol. 1, pp. 998–1007, 2000.